PNAS
www.pnas.org

Supporting Information for:

Remarkable nucleation and growth of ultrafine particles from vehicular exhaust

Song Guo[a,1], Min Hu[a,1,2], Jianfei Peng[b,c,1,3], Zhijun Wu[a], Misti L. Zamora [b,c,1,4], Dongjie Shang[a], Zhuofei Du[a], Jing Zheng[a], Xin Fang[a], Rongzhi Tang[a], Yusheng Wu[a], Limin Zeng[a], Shijin Shuai[d], Wenbin Zhang[d], Yuan Wang[e], Yuemeng Ji[b,c,f], Yixin Li[b,c], Annie L. Zhang[g], Weigang Wang[b,c,h], Fang Zhang[b,c,i], Jiayun Zhao[b,c], Xiaoli Gong[b,c,j], Chunyu Wang[b,c,k], Mario J. Molina[l,2], Renyi Zhang[b,c,2]

This PDF file includes:

Glossary of Acronyms

Calculation of nucleation parameters

Table S1 to S3 (Table S1 through S3 are referenced in the main manuscript)

Figs. S1 to S9 (Figs. S1 through S9 are referenced in the main manuscript)

Glossary of Acronyms

C8-aromatics	Aromatic compounds with eight carbon atoms
C9-aromatics	Aromatic compounds with nine carbon atoms
CO	Carbon oxide
CoagS(D_p)	Coagulation rate of particles with the size of D_p on other particles
CVS	Constant volume sampler
D_m	Mean diameter
DMA-APM	Differential mobility analyzer-aerosol particle mass analyzer
$D_{p,}$	Diameter of newly formed particles
D_p	Diameter of preexisting particles
FR	Formation rate
GR	Growth rate
H_2SO_4	Sulfuric acid
HR-ToF-AMS	High-resolution time-of-flight aerosol mass spectrometer
HTDMA	Hygroscopic tandem differential mobility analyzer
ID-CIMS	Ion drift – chemical ionization mass spectrometry
$J_{3\text{-}25}$	Nucleation fraction of particles within a size range of 3-25 nm
$J(O^1D)$	The photolysis frequency of ozone to yield the excited oxygen atom
k_B	Boltzmann's constant
k_c	Collision rate
K(D_p, D_p')	Coagulation coefficient between particles with diameters of D_p and D_p'
$N_{3\text{-}25}$	Number concentration of particles within a size range of 3-25 nm
NO	Nitrogen oxide
NO_2	Nitrogen dioxide
NO_x	Nitrogen oxides, including nitrogen oxide and nitrogen dioxide
NPF	New particle formation
n(D_p')	Number concentration of preexisting particles
O_3	Ozone
$PM_{2.5}$	Particles with the aerodynamic diameter smaller than 2.5 μm
PKUERS	Peking University atmosphere environment monitoring station
ppb	Parts per billion
PTR-MS	Proton transfer reaction-mass spectrometer
QUALITY	Quasi-atmospheric aerosol evolution study
RH	Relative humidity
SMPS	Scanning mobility particle sizer
SO_2	Sulfur dioxide
UFPs	Ultrafine particles, particles with diameter less than 50 nm
UV	Ultraviolet
VOCs	Volatile organic compounds

Calculation of nucleation parameters

FR is calculated for the nucleation fraction of particles (3-25nm) $J_{3\text{-}25}$, according to (1):

$$J_{3-25} = \frac{dN_{3-25}}{dt} + N_{3-25} * CoagS_8 + F_{growth} \quad (1)$$

where $N_{3\text{-}25}$ is the number concentration of particles within a size range of 3-25 nm, F_{growth} is the flux of particles growing up to over 25 nm, and $CoagS_8$ is the coagulation rate of particles with the diameter of 8 nm, which is the geometric mean of 3-25nm. The coagulation rate is calculated as,

$$\text{Coags}(D_p) = \int K(D_p, D_p')n(D_p')dD_p' \quad (2)$$

where n(D_p') is the number concentration of particles with the size of Dp', and $K(D_p,D_p')$ is the coagulation coefficient between D_p and D_p' particles. The growth rate (*GR*) is calculated as the variation of the mean diameter D_m of the nucleation-mode in unit internal,

$$GR = \frac{\Delta D_m}{\Delta t} \quad (3)$$

We also estimated the coagulation loss rates of freshly-nucleated particles (*SI Appendix*, Table S3), which is dominated by collision loss among freshly-nucleated particles and by coagulation capture of freshly-nucleated particles by large preexisting particles.

Table S1. Experimental conditions of NPF experiments in the QUALITY chamber with initial filtration of preexisting particles. Date, starting time, ambient mass concentration of $PM_{2.5}$ ($\mu g\ m^{-3}$), mixing ratio of NO_x (ppb), mixing ratio of the measured Aromatic VOCs (sum of benzene, toluene, C8 and C9 aromatics in ppb), relative humidity (RH in %), and ozone photolysis frequency $J(O^1D)(s^{-1})$ during the experiment periods, occurrence of ambient NPF (and starting time), formation (*FR* in $cm^{-3}\ s^{-1}$) and growth (*GR* in nm hr^{-1}) rate inside the chamber and in ambient air.

Date	Starting time	$PM_{2.5}$	NO_x	Aromatic VOCs	RH	$J(O^1D)$	Ambient NPF* (starting time)	Chamber		Ambient	
								FR	*GR*	*FR*	*GR*
2013/10/15	9:00	5	14	N.A.	21	6.7×10^{-6}	Y (9:00)	83	42	21	20
2013/10/20	10:30	2	11	2	20	1.3×10^{-5}	Y (10:30)	137	79	26	6
2013/10/23	10:30	9	13	2	14	4.9×10^{-6}	Y (10:00)	266	25	41	12
2013/10/30	13:30	128	46	7	30	1.8×10^{-6}	N	79	7	-	-
2013/11/8	9:00	78	109	N.A.	31	3.1×10^{-6}	N	166	5	-	-
2013/11/12	13:30	2	N.A.	N.A.	19	9.8×10^{-6}	Y (10:30)	326	62	41	16
2013/11/14	12:00	20	9	N.A.	15	4.0×10^{-6}	Y (8:00)	332	15	26	6.
2013/11/16	13:30	12	N.A.	1	16	4.7×10^{-6}	Y	81	25	N.A.	N.A.

* Y – Yes NPF; N – No NPF. N.A. – Data is not available.

Table S2. Experimental conditions for NPF experiments using the QUALITY chamber without initial filtration of preexisting particles. Date, starting time, ambient mass concentration of $PM_{2.5}$ ($\mu g\ m^{-3}$), mixing ratio of NO_x (ppb), mixing ratio of the measured Aromatic VOCs (sum of benzene, toluene, C8 and C9 aromatics in ppb), relative humidity (RH in %), and ozone photolysis frequency $J(O^1D)$ (s^{-1}) during the experiment period, occurrence of ambient NPF, formation (*FR* in $cm^{-3}\ s^{-1}$) and growth (*GR* in nm hr^{-1}) rate inside the chamber.

Date	Starting time	$PM_{2.5}$	NO_x	Aromatic VOCs	RH	$J(O^1D)$	Ambient NPF*	Chamber	
								FR	*GR*
2013/10/28	9:00	275	132	19	52	1.9×10^{-6}	N	29	3
2013/11/1	10:00	264	100	14	49	3.0×10^{-6}	N	34	5
								25	8
								36	12
2013/11/5	10:00	139	88	12	40	3.4×10^{-6}	N	61	9
								90	9
								120	12

* N - No NPF.

Table S3. Collision rate, k_c, Brownian coagulation coefficients, $K(D_p, D_p')$, and coagulation loss rates, Coags(D_p), of freshly-nucleated particles (D_p) by preexisting particles (D_p').

D_p (nm)	D_p' (nm)	k_c [a] ($cm^3\ s^{-1}$)	$K(D_p, D_p')$ [b] ($cm^3\ s^{-1}$)	$n(D_p')$ [c] (cm^{-3})	$\text{Coags}(D_p)$ [d] (s^{-1})
1	1	6.28E-10	6.28E-10	1.00E+08	6.28E-02
1	2	1.06E-09	1.06E-09	2.50E+07	2.65E-02
1	5	4.01E-09	4.01E-09	4.00E+06	1.60E-02
1	10	1.34E-08	1.34E-08	1.00E+06	1.34E-02
1	20	4.90E-08	4.90E-08	2.50E+05	1.22E-02
1	50	2.89E-07	2.89E-07	4.00E+04	1.16E-02
1	100	1.13E-06	1.10E-06	1.00E+04	1.10E-02
1	1000	1.11E-04	3.00E-05	1.00E+02	3.00E-03
1	10000	1.11E-02	2.80E-04	1.00E+00	2.80E-04

[a] The collision rate is estimated using $k_c = \pi(D_p + D_p')^2 \times (8k_BT/\pi\mu)^{1/2}$, where $\mu = (m_p \times m_{p'})/ (m_p + m_{p'})$, k_B is the Boltzmann's constant, and m_p and $m_{p'}$ are the masses for freshly-nucleated and preexisting particles, respectively. The particle density is assumed to be 1g cm^{-3}.

[b] The Brownian coagulation coefficients are calculated using the Fuchs' flux formula (5).

[c] The number concentration of preexisting particles is estimated from data in Fig. 2, the number concentration for freshly-nucleated particles is estimated assuming that the particle surface area is invariant, with a value of about 314 $\mu m^2\ cm^{-3}$ for all cases, compared to those from 1000 to 2500 in Fig. 2B.

[d] The coagulation rate of freshly-nucleated particles is estimated as $\text{Coags}(D_p) = K(D_p, D_p') \times n(D_p')$.

For freshly nucleated particles, the particle coagulation falls into the free molecular regime (5). The coagulation loss among freshly-nucleated particles ($\text{Coags}(D_p)$) is proportional to $D_p^{1/2} \times n_p$, where D_p and n_p is the size and number concentration of freshly-nucleated particles, respectively. The coagulation loss of freshly-nucleated particles by existing particles (D_p' <100 nm) is proportional to $D_p'^2 \times n_p$', where D_p' and n_p' are the size and number concentration of existing particles, respectively. Hence, the coagulation loss among freshly-nucleated particles is dependent on the number concentration of freshly-nucleated particles, while coagulation loss of freshly-nucleated particles by existing particles is dependent on the surface area and number concentration of existing particles.

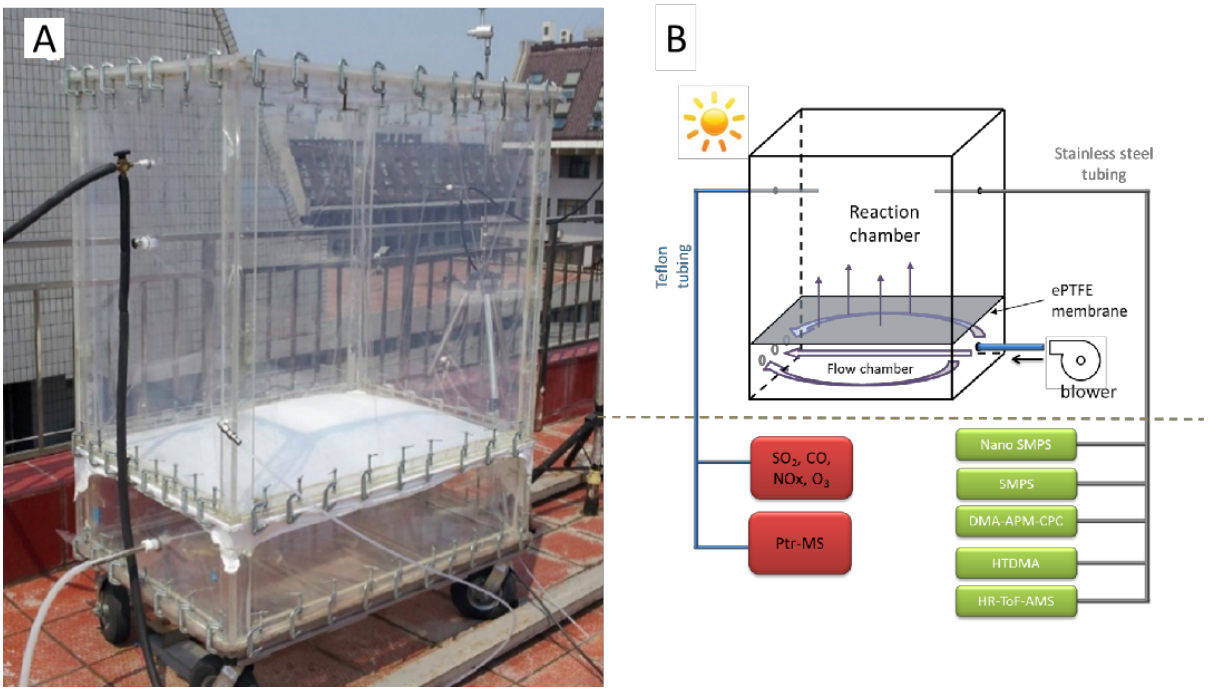

Fig. S1. The QUALITY chamber. (**A**) Deployment of the QUALITY at the PKUERS site. (**B**) Schematic representation of the chamber setup.

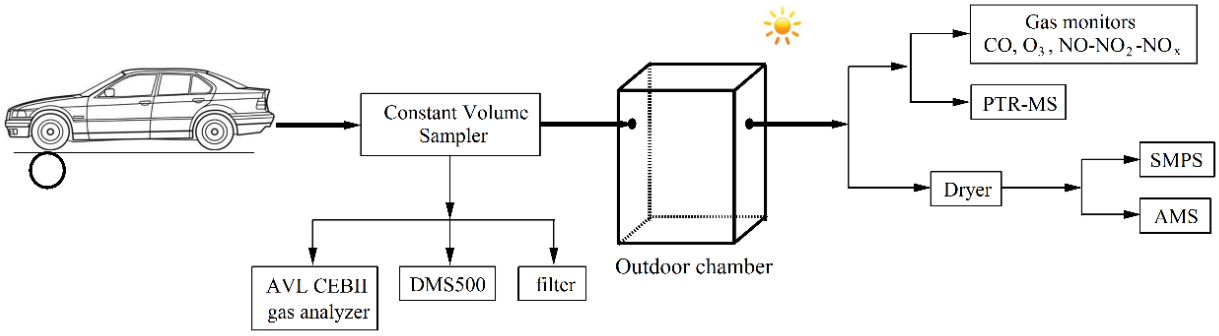

Fig. S2. Schematic of the gasoline vehicle exhaust experiments. PTR-MS for proton transfer – reaction mass spectrometer; SPMS for scanning mobility particle sizer; and AMS for aerosol mass spectrometer.

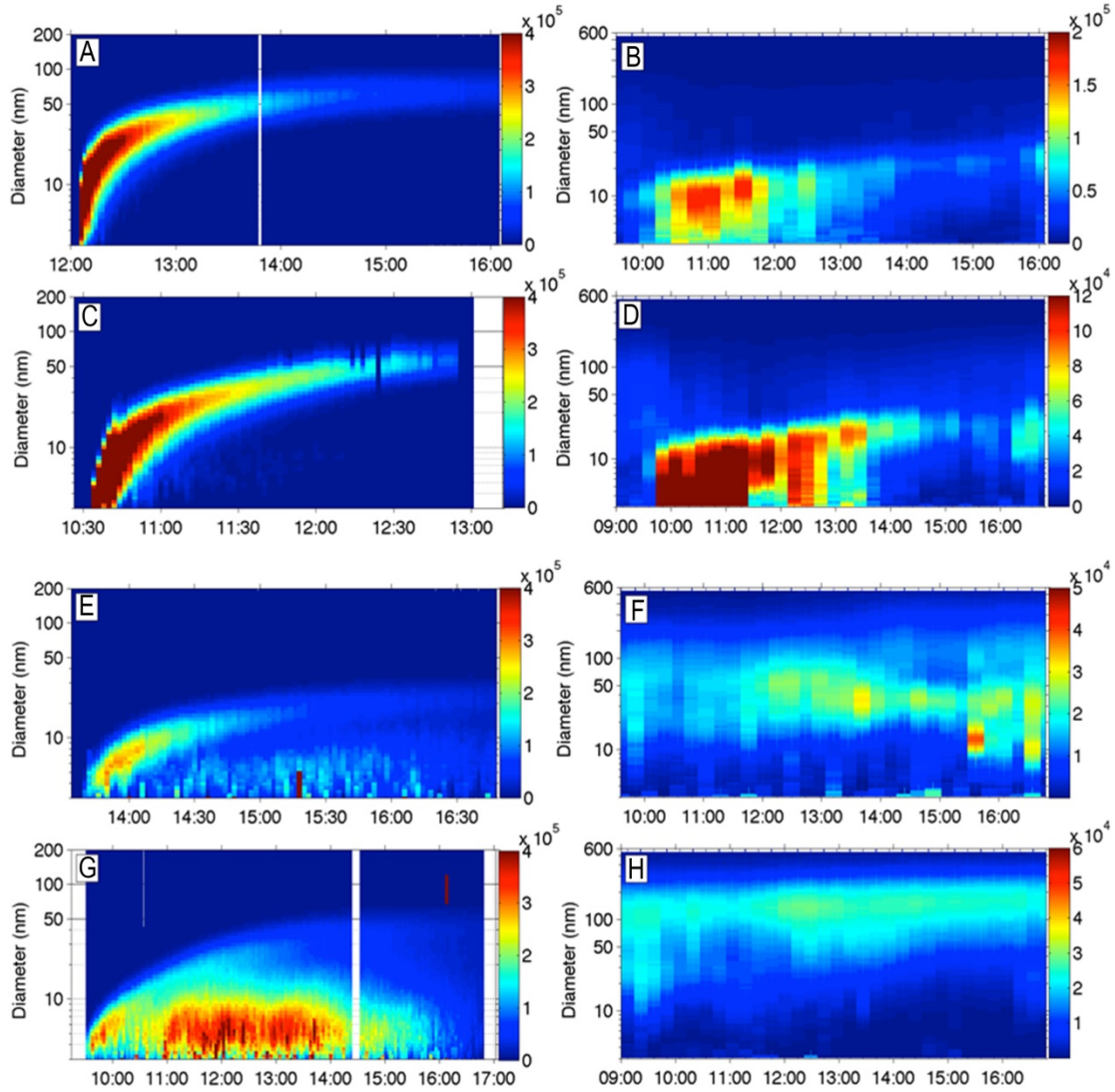

Fig. S3. Particle number size distributions inside the QUALITY chamber (left) and in ambient air (right). (**A, C, E** and **G**) Inside the chamber, NPF occurred consistently on both clean (October 20, 2013, A; October 23, 2013, B) and polluted days (October 30, 2013, E; November 8, 2013, G). (**B**, **D**, **F** and **H)** In the ambient air, NPF occurred on clean days (October 20, 2013, B; October 23, 2013, D), but not on polluted days (October 30, 2013, F; November 8, 2013, H).

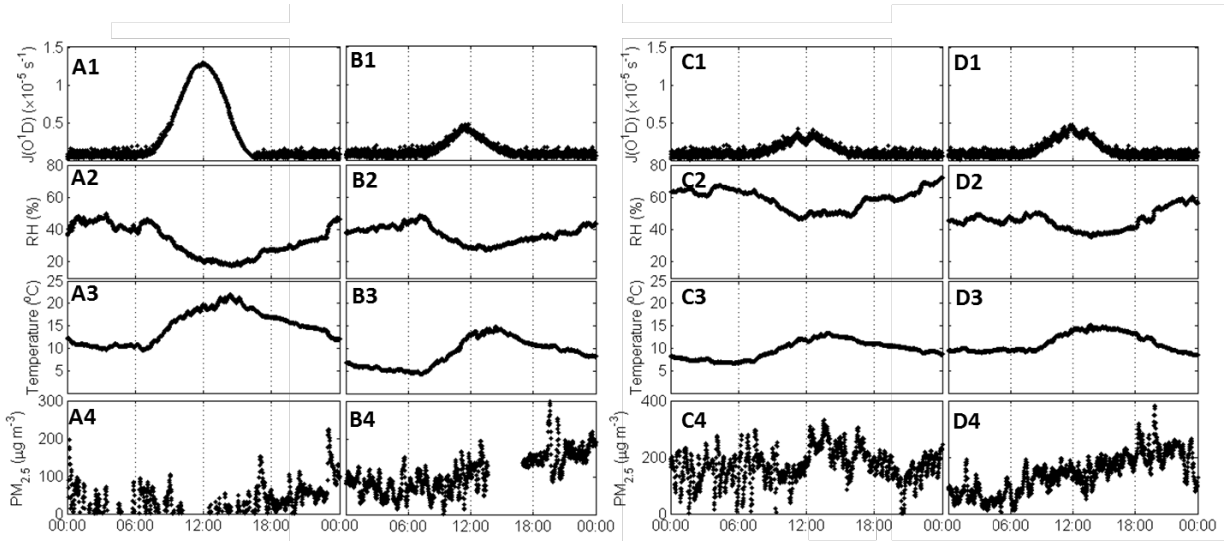

Fig. S4. Ambient measurements of ozone photolysis frequency $J(O^1D)$, relative humidity (RH), temperature, and $PM_{2.5}$ during NPF experiments. (**A1** to **A4**) With initial filtration on October 23, 2013 (clean). (**B1** to **B4**) With initial filtration on November 8, 2013 (hazy). (**C1** to **C4**) Without initial filtration on November 1, 2013 (clean). (**D1** to **D4**) Without initial filtration on November 5, 2013 (polluted).

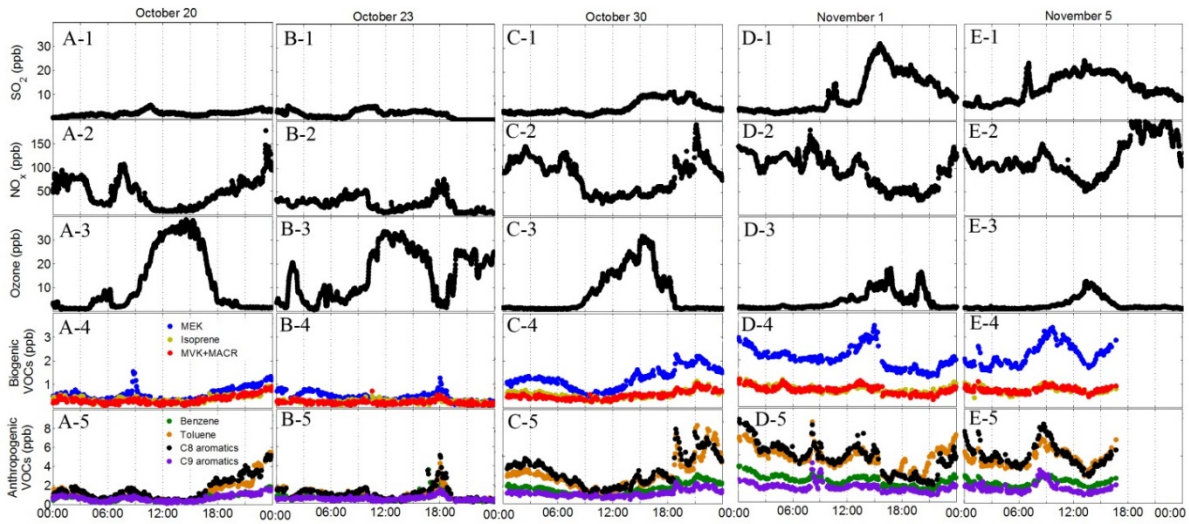

Fig. S5. Ambient gas concentrations during QUALITY chamber experiments. (**A1** to **A4**) With initial particle filtration on October 20, 2013 (clean). (**B1** to **B4**) With initial particle filtration on October 23, 2013 (hazy). (**C1** to **C4**) Without initial filtration on October 30 (clean). (**D1** to **D4**) Without initial filtration on November1, 2013 (hazy). (**E1** to **E4**) Without initial filtration on November 5, 2013 (polluted).

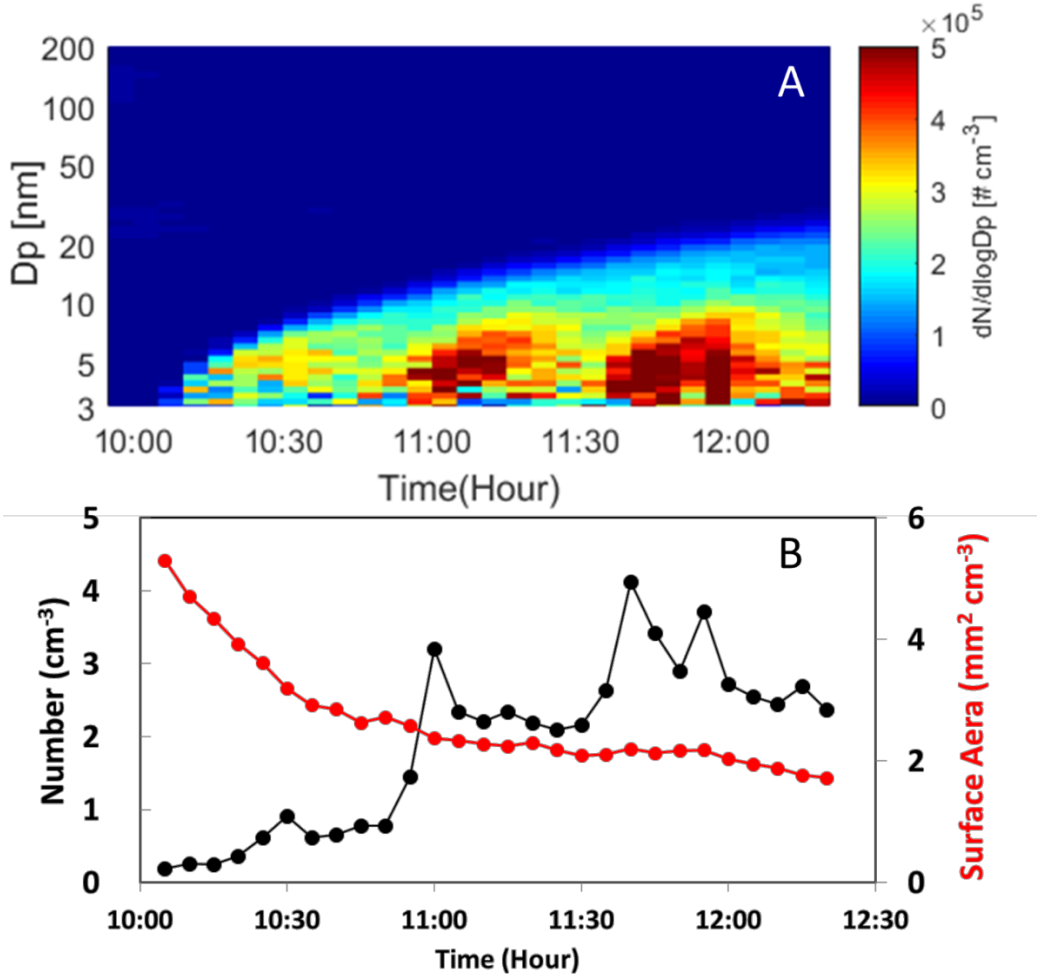

Fig. S6. QUALITY chamber experiments without initial particle filtration. (**A**) Particle number size distribution. (**B**) Total number concentration and surface area during the dilution experiments on November 5, 2013 (polluted).

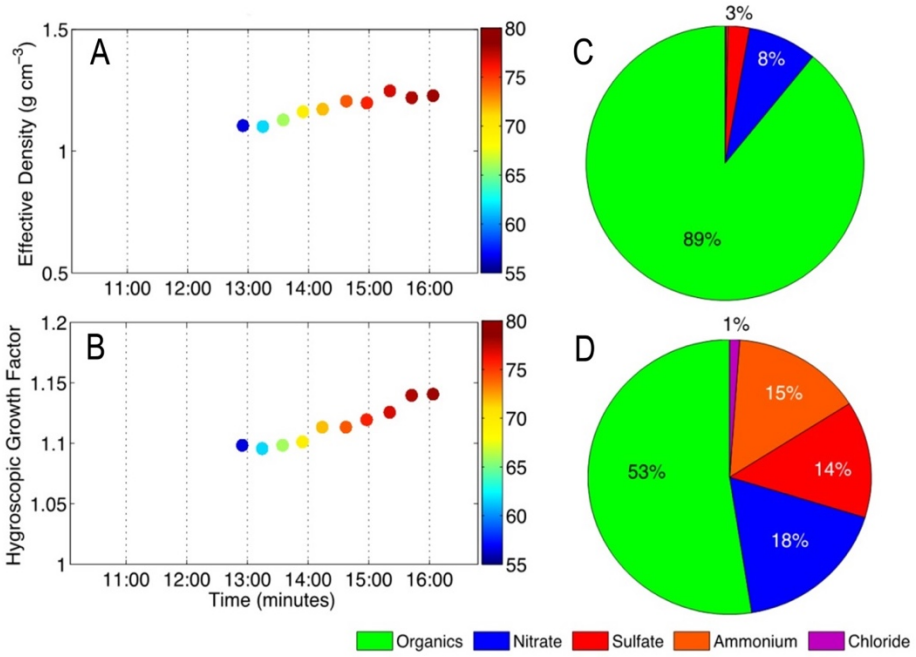

1

Fig. S7. Inferring the chemical composition of nanoparticles. (**A**) Size and temporally resolved effective density. (**B**) Size and temporally resolved hygroscopicity. (**C** and **D**) Chemical composition for particles with a mean particle size of 55 nm (C) and 80 nm (D). All experiments were carried on October 23, 2013.

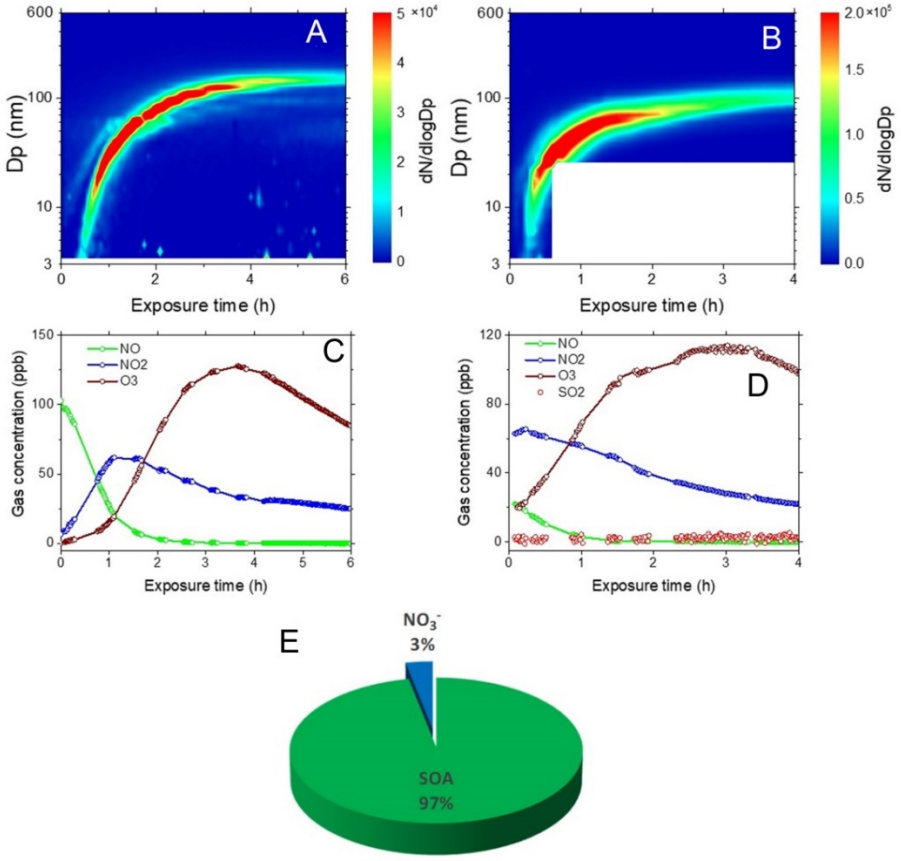

Fig. S8. NPF from vehicular exhaust. (**A** and **B**) Particle number size distributions during two experiments upon exposure of vehicular exhaust. (**C** and **D**) Evolutions in the concentrations of NO (green), NO_2 (blue), O_3 (brown) and SO_2 (red) correspond to the experiments (A) and (B), respectively. The initial O_3 concentrations are 0 and 80 ppb in A and B, leading to distinct NPF and photochemistry between the two experiments. (**E**) Mass fraction of secondary organic aerosols (SOA, green) and nitrate (blue) measured by HR-ToF-AMS.

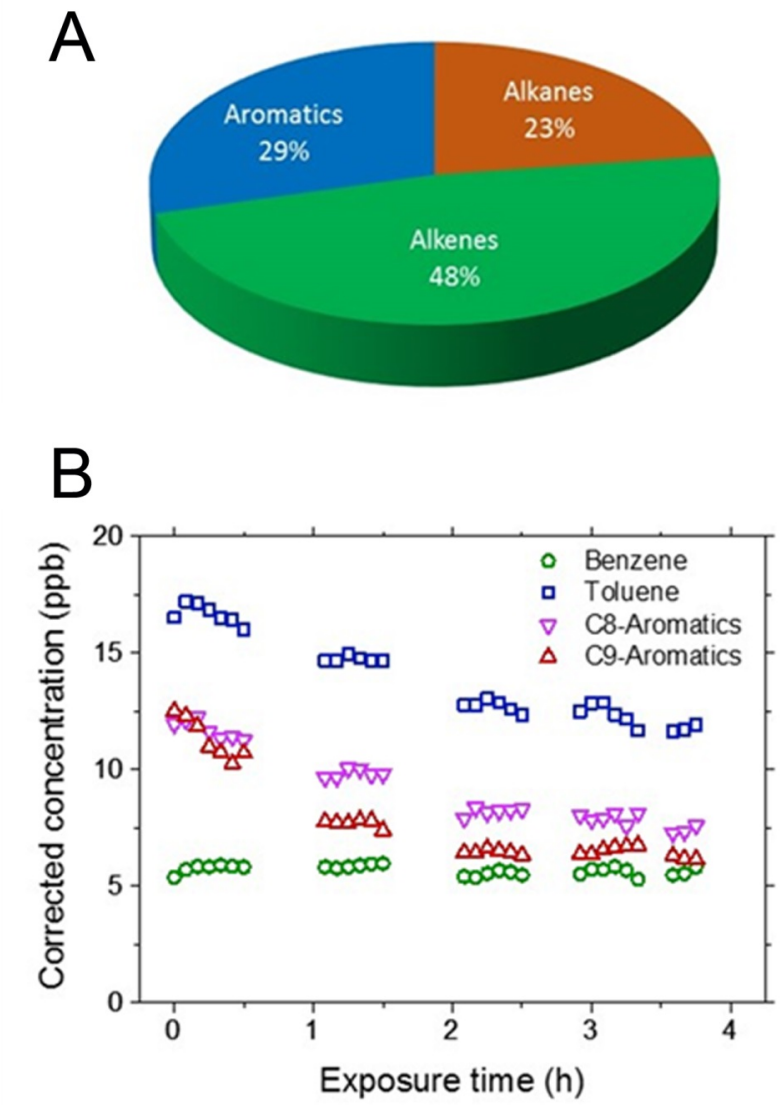

Fig. S9. Significant aromatic VOCs from vehicular exhaust. (**A**) Fraction of VOCs from vehicular exhaust inside the chamber. (**B**) Evolution of aromatics upon exposure of vehicular exhaust inside the chamber.